

Received 21 December 2020; revised 17 February 2021; accepted 19 February 2021. Date of publication 24 February 2021; date of current version 11 March 2021.

Digital Object Identifier 10.1109/OJAP.2021.3061935

Antenna Array Calibration Using a Sparse Scene

JOHANNA GEISS^{ID} (Graduate Student Member, IEEE), ERIK SIPPEL^{ID},
MARKUS HEHN^{ID} (Graduate Student Member, IEEE), AND MARTIN VOSSIEK^{ID} (Fellow, IEEE)

Institute of Microwaves and Photonics, Friedrich-Alexander University Erlangen-Nuremberg, 91058 Erlangen, Germany

CORRESPONDING AUTHOR: J. GEISS (e-mail: johanna.geiss@fau.de)

This work was supported by Analog Devices/Symeo GmbH/München, Germany.

ABSTRACT In radar systems, antenna arrays acquire direction-dependent information to localize targets or create images of the environment. However, because of unknown complex amplitudes per channel and mutual coupling, a calibration is necessary for good performance. Common calibration approaches measure to targets under known angles in a multipath-free far-field environment, which often can only be provided by anechoic chambers. Therefore, this process is not suitable for low-cost and frequent calibration. To overcome these limitations, this paper proposes a novel calibration approach using an unknown but sparse target scene. Multiple measurements at known relative positions of the radar are combined to a synthetic aperture. Then, the full mutual coupling matrix is estimated simultaneously with the unknown target scene. The method requires neither target position information, far-field conditions, nor an anechoic chamber because multipath propagation can be suppressed easily for targets located in the near-field. The proposed calibration approach is validated by measurements of a commercial 77 GHz radar. The performance is evaluated by comparing the achieved image quality using the calibration results of this work and the radar's ex-factory calibration data. The proposed novel calibration procedure improves the image quality, while considerably lowering the demands on the calibration measurements and environment.

INDEX TERMS Antenna array, calibration, compressed sensing, mutual coupling, radar, sparsity.

I. INTRODUCTION

TODAY, radar sensors are a key technology in many different fields such as the automotive sector [1], robotic applications [2], medical engineering [3], microwave imaging, e.g., in security applications [4], and spaceborne radar [5]. In order to achieve a spatial resolution for radar imaging or angle-of-arrival (AOA) estimation, synthetic aperture radars (SAR) [6], or antenna arrays in single-input multiple-output (SIMO), and multiple-input multiple-output (MIMO) systems are used [7]. However, the performance of systems using antenna arrays is generally impaired by unknown gain and phase errors per channel. Additionally, mutual coupling occurs between the channels, when antennas are arranged closely to each other, which is usually the case in order to reach unambiguous angle estimation [8]. These impairments have a severe impact on the radar's performance [9], [10]. Hence, the calibration of a radar sensor is a standard procedure before its initial operation [8], [11].

The standard calibration approach of complex gains and mutual coupling is to perform calibration measurements to

targets at known locations [12]–[14]. However, the determination of the absolute position of a calibration target relative to the sensor puts high demands on the reference system. Therefore, common approaches work in the far-field of the array and hence only require the knowledge of the target's angle relative to the sensor [12], [13], [15]. This angle can be acquired approximately by rotating the radar around the antenna center. Hence, a less accurate reference positioning system for the target is necessary [15]. However, in order to match the far-field condition, the demands on the calibration setup increase. Therefore, most calibrations are performed in anechoic chambers which yield controlled far-field environments [8] without multipath propagation, avoiding calibration errors [11].

Other calibration approaches as in [16]–[20] perform blind calibration, i.e., with unknown source positions. However, they do not compensate mutual coupling, thereby reducing the number of calibration parameters. References [21], [22] present online calibration approaches, simultaneously estimating the unknown parameters and the desired measurement

result. Blind and on-line approaches, however, are generally ill-conditioned because they only use information of a single measurement to estimate a comparatively large number of unknowns. Hence, they are only suitable for small calibration errors and favorable measurement conditions [8].

In many radar applications the target scene can be assumed to be sparse. Sparsity is exploited in compressed sensing (CS) techniques, which were first introduced in [23], [24], and have been applied to radar systems to reduce the amount of data [25] or to create high resolution images [26]. Recently, CS has also been applied to calibration. In [6], [27]–[29], sparsity was exploited to calibrate complex gains using targets under unknown angles. Mutual coupling was considered for on-line calibration in [30] and [31]. However, these works also assumed angle measurements, thereby implying multipath free far-field conditions. Also, the unknown angles can only be estimated up to an arbitrary rotation factor, because a progressive phase factor in the coupling matrix is interchangeable with an angle rotation [17]. Furthermore, in these works, no measurements were performed to verify the approaches. Although sparsity relaxes the calibration problem, estimating unknown directional angles and mutual coupling simultaneously using a single measurement will still lead to a poorly conditioned estimation problem, which is unlikely to perform reliably in most real-world scenarios.

Therefore, a low effort calibration procedure is necessary, which does neither require excessive multipath free far-field conditions, and hence an anechoic chamber, nor a reference system providing the target positions relative to the radar. E.g., [32] formulates the need for a quick end-of-line in-situ calibration of automotive radar sensors. Also, [33] states that re-calibration to maintain the radar sensor's peak performance is typically not done, because the calibration effort is too high.

In order to overcome the limitations of common approaches, we propose a low-effort near-field calibration for radar systems using a sparse but unknown target scene. This calibration significantly lowers the requirements on a multipath free environment and can therefore be performed in most arbitrary environments. By performing multiple measurements at different known relative positions of either the radar or the sparse scene, a synthetic aperture [34] is created, providing the necessary information for calibration. Thereby, a sufficiently well conditioned problem is created, while only requiring information about the relative movement yielding the synthetic aperture but no information about the target positions relative to the radar. The proposed calibration procedure is validated by measurements using a commercially available radar sensor in an indoor environment, without using an anechoic chamber. The calibration is shown to yield improved imaging performance compared to the sensor's ex factory calibration, whereas the requirements on the measurement setup are significantly reduced.

In this paper, the calibration is derived for the widely used frequency modulated continuous wave (FMCW) radar. Note,

however, that the same approach can be used for other standard radar types, such as the orthogonal frequency-division multiplexing (OFDM) radar.

The remainder of this paper is organized as follows: The system model for a FMCW radar including mutual coupling is derived in Section II. In Section III, the proposed calibration is described and interpreted. Furthermore, a problem relaxation for uniform linear arrays is discussed. The measurement setup to validate the concept in a real world indoor setting as well as the calibration results are shown in Section IV, followed by a conclusion.

II. SYSTEM MODEL

In this section, the signal model for the widely used FMCW radar is presented. The FMCW radar principle allows estimating range, angle, and velocity with good accuracy, while the necessary hardware architecture is comparatively simple. Therefore, it is used in many applications, and especially most automotive radar sensors are based on the FMCW principle [35], [36].

At first, the ideal case is considered, then the case including complex gains and mutual coupling is derived and shown to be approximately equivalent to the ideal case multiplied by a coupling matrix. For a concise representation, a SIMO radar system comprising a single transmit (TX) channel and N_{RX} coherent receive (RX) channels is considered. Furthermore, for simplification, the problem is limited to the 2D case. The extension to a MIMO radar system comprising multiple TX channels as well as the 3D case is straightforward. An overview of the measurement model is illustrated in Fig. 1.

For the measurement process, we assume a radar located at the position $\mathbf{p}_{n_p} = (x_{n_p}, y_{n_p})^T$, with $1 \leq n_p \leq N_p$ and N_p as the number of totally performed measurements. The radar comprises one TX antenna, located at the position $\mathbf{p}_{TX} = (x_{TX}, y_{TX})^T$, and N_{RX} RX antennas at the positions $\mathbf{p}_{n_{RX}} = (x_{n_{RX}}, y_{n_{RX}})^T$, with $1 \leq n_{RX} \leq N_{RX}$. All antenna positions are given with respect to the radar center. The measurement procedure begins with the TX antenna emitting the linearly frequency-modulated transmit signal

$$s^{tx}(t) = A_{TX} \cos\left(2\pi\left(f_0 + \frac{1}{2}\mu t\right)t\right) \text{rect}\left(\frac{t - 0.5T}{T}\right), \quad (1)$$

with the time t , the signal amplitude A_{TX} , the carrier frequency f_0 , the sweep duration T and the sweep-rate $\mu = \frac{B}{T}$, where B denotes the sweep bandwidth. The rectangular function $\text{rect}(x)$ is given by

$$\text{rect}(x) = \begin{cases} 1, & \text{if } -\frac{1}{2} < x \leq \frac{1}{2} \\ 0, & \text{otherwise.} \end{cases} \quad (2)$$

The signal is scattered at a target n_T at position $\mathbf{p}_{n_T} = (x_{n_T}, y_{n_T})^T$, which is considered a point target, and reflected back to the radar's RX antenna array, as illustrated in Fig. 1.

A. IDEAL SYSTEM MODEL

For now, all influences like unknown channel attenuation and phase shift, and mutual coupling are neglected. The

resulting ideal signals will be marked by the superscript id. At the measurement position n_p , the ideal signal at the n_{RX} th antenna, which is received after the reflection of the transmit signal at the n_T th target is given by

$$s_{n_p, n_{RX}, n_T}^{rx, id}(t) = A_{n_p, n_{RX}, n_T} \cos\left(2\pi\left(f_0 + \frac{1}{2}\mu(t - \tau_{n_p, n_{RX}, n_T})\right)\right) \times \text{rect}\left(\frac{t - 0.5T}{T}\right), \quad (3)$$

with the delay

$$\tau_{n_p, n_{RX}, n_T} = \frac{d_{TX \rightarrow n_T, n_p} + d_{n_T \rightarrow n_{RX}, n_p}}{c_0}, \quad (4)$$

where c_0 denotes the speed of light,

$$d_{TX \rightarrow n_T, n_p} = \|\mathbf{p}_{n_T} - (\mathbf{p}_{n_p} + \mathbf{p}_{TX})\|_2, \quad (5)$$

denotes the distance from the TX antenna to the n_T th target, and

$$d_{n_T \rightarrow n_{RX}, n_p} = \|(\mathbf{p}_{n_p} + \mathbf{p}_{n_{RX}}) - \mathbf{p}_{n_T}\|_2 \quad (6)$$

denotes the distance from the n_T th target to the n_{RX} th RX antenna, see Fig. 1. The receive signal's amplitude

$$A_{n_p, n_{RX}, n_T} = A_{TX} a_{TX \rightarrow n_T \rightarrow n_{RX}, n_p} \quad (7)$$

consists of the path attenuation

$$a_{TX \rightarrow n_T \rightarrow n_{RX}, n_p} = \frac{1}{d_{TX \rightarrow n_T, n_p} d_{n_T \rightarrow n_{RX}, n_p}}, \quad (8)$$

and an unknown, possibly complex backscatter cross section A_{n_T} of the target. Amplitude variations caused by directional antenna characteristics are omitted.

For a number of N_T point targets, the individual reflected and received signals $s_{n_p, n_{RX}, n_T}^{rx, id}(t)$ are superposed linearly at the antenna, yielding the ideal radio frequency receive signal as

$$s_{n_p, n_{RX}}^{rx, id}(t) = \sum_{n_T=1}^{N_T} s_{n_p, n_{RX}, n_T}^{rx, id}(t). \quad (9)$$

Note that this does not put any limitations on the target scene, since all scenes can be represented as a possibly infinite sum of point targets.

The receive signal is then mixed into the baseband using the original transmit signal (1) and by low-pass filtering the result to suppress the signal components at the double carrier frequency, see Fig. 1, yielding the ideal baseband receive signal

$$s_{n_p, n_{RX}}^{id}(t) = s^{tx}(t) \sum_{n_T=1}^{N_T} s_{n_p, n_{RX}, n_T}^{rx, id}(t) \approx \sum_{n_T=1}^{N_T} A_{n_p, n_{RX}, n_T}$$

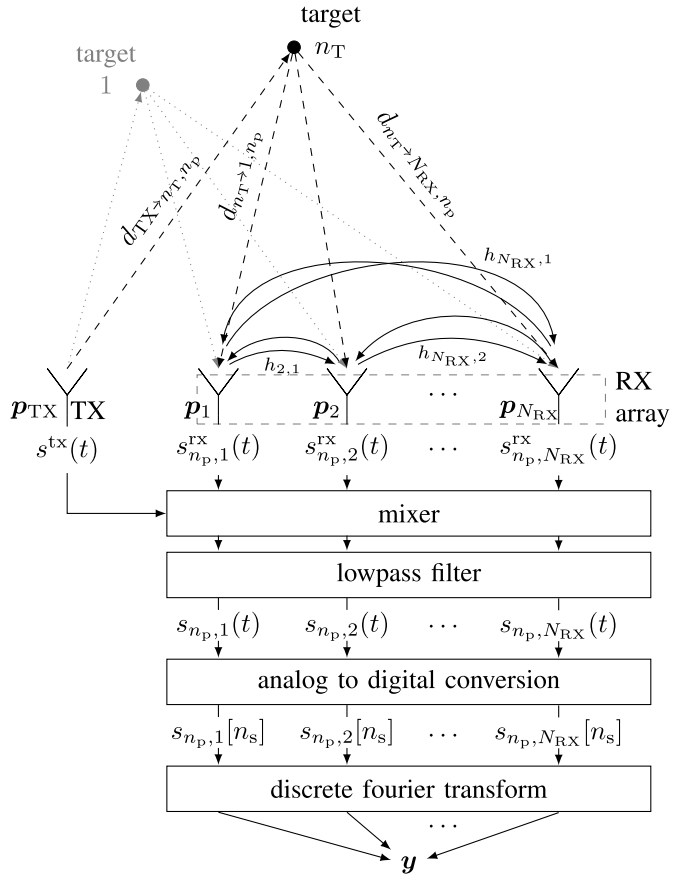


FIGURE 1. Schematic diagram of the measurement model including mutual coupling and the signal processing.

$$\times \cos(2\pi\mu\tau_{n_p, n_{RX}, n_T} t + 2\pi f_0 \tau_{n_p, n_{RX}, n_T}) \times \text{rect}\left(\frac{t - 0.5T}{T}\right), \quad (10)$$

where the amplitude factors resulting from the mixing process are included into the transmit signal's amplitude A_{TX} in (7). Furthermore, the shift and compression of the rectangular function resulting from the time delay as well as signal components containing the squared delay can be neglected as long as $\tau_{n_p, n_{RX}, n_T} \ll T$ holds. Transforming the ideal baseband signal into the frequency domain and considering the analytic representation of the signal with only positive frequencies yields

$$S_{n_p, n_{RX}}^{id}(f) = \sum_{n_T=1}^{N_T} T A_{n_p, n_{RX}, n_T} \times e^{j2\pi f_0 \tau_{n_p, n_{RX}, n_T}} e^{-j\pi(f - \mu\tau_{n_p, n_{RX}, n_T})T} \times \text{sinc}((f - \mu\tau_{n_p, n_{RX}, n_T})T). \quad (11)$$

Note that the measurement signal in the frequency domain comprises sinc functions at the so called beat-frequencies $\mu\tau_{n_p, n_{RX}, n_T}$, which depend on the total delay caused by a

target. Therefore, the frequency axis is equivalent to a delay-axis and thereby a range-axis.

In the radar, the baseband signal in the time domain (10) is sampled with a sampling frequency f_s . For a discrete sampling point n_s with $0 \leq n_s < N_s$ and $N_s = T f_s$, the analytic representation of the baseband signal (10) at a single antenna at the time instance $t = n_s \frac{1}{f_s}$ can be written as

$$s_{n_p, n_{RX}}^{\text{id}}[n_s] = \sum_{n_T=1}^{N_T} A_{n_p, n_{RX}, n_T} \times e^{j2\pi(\mu \tau_{n_p, n_{RX}, n_T} n_s \frac{T}{N_s} + f_0 \tau_{n_p, n_{RX}, n_T})}. \quad (12)$$

Using (7), this can now be expressed in matrix notation as a signal matrix $S_{n_p, N_{RX}}^{\text{id}}$ and a vector \mathbf{x} containing the complex reflection coefficients A_{n_T} of the targets, such that

$$\begin{aligned} s_{n_p, n_{RX}}^{\text{id}} &= S_{n_p, n_{RX}}^{\text{id}} \mathbf{x} \\ &= \begin{pmatrix} s_{n_p, n_{RX}, 1}^{\text{id}}[0] & \cdots & s_{n_p, n_{RX}, N_T}^{\text{id}}[0] \\ \vdots & \ddots & \vdots \\ s_{n_p, n_{RX}, 1}^{\text{id}}[N_s - 1] & \cdots & s_{n_p, n_{RX}, N_T}^{\text{id}}[N_s - 1] \end{pmatrix} \begin{pmatrix} A_1 \\ \vdots \\ A_{N_T} \end{pmatrix}, \end{aligned} \quad (13)$$

with the entries of $S_{n_p, n_{RX}}^{\text{id}}$

$$s_{n_p, n_{RX}, n_T}^{\text{id}}[n_s] = a_{TX \rightarrow n_T \rightarrow n_{RX}, n_p} \times e^{j2\pi(\mu \tau_{n_p, n_{RX}, n_T} n_s \frac{T}{N_s} + f_0 \tau_{n_p, n_{RX}, n_T})}, \quad (14)$$

where $a_{TX} = 1$ is assumed for simplicity. Using the discrete Fourier transform (DFT), $S_{n_p, n_{RX}}^{\text{id}}$ can be transformed into the frequency domain using a single matrix multiplication

$$S_{n_p, n_{RX}}^{\text{DFT,id}} = \mathbf{W} S_{n_p, n_{RX}}^{\text{id}} = \begin{pmatrix} \mathbf{h}_{n_p, n_{RX}, 1}^T \\ \vdots \\ \mathbf{h}_{n_p, n_{RX}, N_s}^T \end{pmatrix}, \quad (15)$$

with the quadratic DFT matrix \mathbf{W} , whose (i, j) th entry is given by $\frac{1}{\sqrt{N_s}} \omega^{(i-1)(j-1)}$, with $\omega = e^{-j\frac{2\pi}{N_s}}$. Note that the DFT matrix is a unitary matrix, and therefore preserves all information as well as the signal energy. In this representation, the rows $\mathbf{h}_{n_p, n_{RX}, n_s}^T$ of the resulting matrix describe the influence of all targets, with amplitudes stored in \mathbf{x} , on the baseband signal's n_s th frequency bin, and thereby on a particular range bin. Therefore, the frequency domain analysis enables an easy discarding of unwanted range areas from the following signal processing by omitting the corresponding rows from $S_{n_p, n_{RX}}^{\text{DFT,id}}$.

Considering all antennas and rearranging the rows $\mathbf{h}_{n_p, n_{RX}, n_s}^T$ of (15), we can form an ideal measurement matrix for a single radar position

$$\mathbf{H}_{n_p} = \begin{pmatrix} \mathbf{H}'_{n_p, 1} \\ \vdots \\ \mathbf{H}'_{n_p, N_s} \end{pmatrix} \text{ with } \mathbf{H}'_{n_p, n_s} = \begin{pmatrix} \mathbf{h}_{n_p, 1, n_s}^T \\ \vdots \\ \mathbf{h}_{n_p, N_T, n_s}^T \end{pmatrix}. \quad (16)$$

When measurements at multiple radar positions n_p are available, the corresponding \mathbf{H}_{n_p} can be stacked to get the full measurement matrix \mathbf{H} . Then, the complete ideal measurement process can be described as a linear operation

$$\mathbf{y}_{\text{id}} = \mathbf{H} \mathbf{x}, \quad (17)$$

with the stacked Fourier transformed ideal measurement data $\mathbf{y}_{\text{id}} \in \mathbb{C}^{N_p N_{RX} N_s}$.

B. MUTUAL COUPLING SIGNAL MODEL

In the following, the non-ideal case including mutual coupling and channel mismatches is considered. Coupling occurs when a part of the signal impinging on the n'_{RX} th antenna (9) is reflected and received by the n_{RX} th antenna, as described by a transfer function $h_{n_{RX}, n'_{RX}}(t)$ [14], see Fig. 1. $h_{n_{RX}, n'_{RX}}(t)$ represents the channel's own distortion resulting from small hardware deviations at the different channels. The receive signal including mutual coupling can then be stated as the convolution, denoted by the operator $*$, of the transfer function with the ideal impinging signals (9), yielding [14]

$$\begin{aligned} s_{n_p, n_{RX}}^{\text{rx}}(t) &= \sum_{n'_{RX}=1}^{N_{RX}} \sum_{n_T=1}^{N_T} h_{n_{RX}, n'_{RX}} * s_{n_p, n'_{RX}, n_T}^{\text{rx,id}}(t) \\ &= \sum_{n'_{RX}=1}^{N_{RX}} \sum_{n_T=1}^{N_T} \int_0^\infty h_{n_{RX}, n'_{RX}}(\tau) s_{n_p, n'_{RX}, n_T}^{\text{rx,id}}(t - \tau) d\tau, \end{aligned} \quad (18)$$

and the mixed signal follows, similarly to (10), as

$$\begin{aligned} s_{n_p, n_{RX}}(t) &\approx \sum_{n'_{RX}=1}^{N_{RX}} \sum_{n_T=1}^{N_T} A_{n_p, n_{RX}, n_T} \int_0^\infty h_{n_{RX}, n'_{RX}}(\tau) \\ &\quad \times \cos(2\pi\mu t(\tau_{n_p, n'_{RX}, n_T} + \tau)) \\ &\quad + 2\pi f_0(\tau_{n_p, n'_{RX}, n_T} + \tau)) \\ &\quad \times \text{rect}\left(\frac{t - 0.5T}{T}\right) d\tau. \end{aligned} \quad (19)$$

Here, again, the shift and compression of the rectangular function caused by the additional delay τ have been neglected, because for small antenna arrays the length of the transfer function is significantly shorter than T .

For the trivial case of $h_{n_{RX}, n'_{RX}}(t) = 0$ for $n_{RX} \neq n'_{RX}$ and $h_{n_{RX}, n_{RX}}(t) = \delta(t)$, with the delta distribution $\delta(t)$, the signals (18) and (19) correspond to (9) and (10) respectively, describing the ideal signals as a special case of mutual coupling.

As in the ideal case, (19) is now sampled in the radar to acquire the discrete signal $s_{n_p, n_{RX}}[n_s]$, see Fig. 1. However, for a better understanding, we will proceed using the continuous signal. Transforming the analytic signal representation of the baseband signal (19) into the frequency domain leads to

$$\begin{aligned}
 S_{n_p, n_{RX}}(f) &= \sum_{n_{RX}=1}^{N_{RX}} \sum_{n_T=1}^{N_T} A_{n_p, n_{RX}, n_T} \int_0^\infty h_{n_{RX}, n'_{RX}}(\tau) \\
 &\quad \times \delta(f - \mu(\tau_{n_p, n_{RX}, n_T} + \tau)) e^{j2\pi f_0(\tau_{n_p, n_{RX}, n_T} + \tau)} \\
 &\quad * T \operatorname{sinc}(fT) e^{-j\pi fT} d\tau \\
 &= \sum_{n_{RX}=1}^{N_{RX}} \sum_{n_T=1}^{N_T} A_{n_p, n_{RX}, n_T} \int_0^\infty h_{n_{RX}, n'_{RX}}(\tau) \\
 &\quad \times T e^{j2\pi f_0(\tau_{n_p, n_{RX}, n_T} + \tau)} e^{-j\pi(f - \mu(\tau_{n_p, n_{RX}, n_T} + \tau))T} \\
 &\quad \times \operatorname{sinc}((f - \mu(\tau_{n_p, n_{RX}, n_T} + \tau))T) d\tau, \quad (20)
 \end{aligned}$$

which is the equivalent of (11) including coupling.

Because multiple antennas and targets superpose linearly, for simplicity the case is now reduced to a single radar position, a single target n_T and a single antenna pair (n_{RX}, n'_{RX}) , with the corresponding delays $\tau_{n_{RX}}$ and $\tau_{n'_{RX}}$. Furthermore, it is assumed that mutual coupling is dominated by the direct reflection from antenna n'_{RX} to antenna n_{RX} , which is characterized by an amplitude factor $c_{n_{RX}, n'_{RX}}$ and a time delay $\Delta\tau$. Hence, coupling effects resulting from multiple reflections can be discarded and the transfer functions can be stated as $h_{n_{RX}, n_{RX}}(t) = c_{n_{RX}, n_{RX}} \delta(t)$ and $h_{n_{RX}, n'_{RX}}(t) = c_{n_{RX}, n'_{RX}} \delta(t - \Delta\tau)$, where $\Delta\tau \approx d_{n_{RX}, n'_{RX}}/c_0$, with the antenna to antenna distance $d_{n_{RX}, n'_{RX}}$. Assuming $A_{n_p, n_{RX}, n_T} = 1$, (20) can be reduced to

$$\begin{aligned}
 S_{n_{RX}}(f) &= c_{n_{RX}, n_{RX}} T e^{j2\pi f_0 \tau_{n_{RX}}} e^{-j\pi(f - \mu \tau_{n_{RX}})T} \\
 &\quad \times \operatorname{sinc}((f - \mu \tau_{n_{RX}})T) + c_{n_{RX}, n'_{RX}} T e^{j2\pi f_0(\tau_{n'_{RX}} + \Delta\tau)} \\
 &\quad \times e^{-j\pi(f - \mu(\tau_{n'_{RX}} + \Delta\tau))T} \\
 &\quad \times \operatorname{sinc}((f - \mu(\tau_{n'_{RX}} + \Delta\tau))T) \\
 &\stackrel{(a)}{\approx} c_{n_{RX}, n_{RX}} T e^{j2\pi f_0 \tau_{n_{RX}}} e^{-j\pi(f - \mu \tau_{n_{RX}})T} \\
 &\quad \times \operatorname{sinc}((f - \mu \tau_{n_{RX}})T) + c_{n_{RX}, n'_{RX}} T e^{j\pi(2f_0 + \mu T)\Delta\tau} \\
 &\quad \times e^{j2\pi f_0 \tau_{n'_{RX}}} e^{-j\pi(f - \mu \tau_{n'_{RX}})T} \operatorname{sinc}((f - \mu \tau_{n'_{RX}})T) \\
 &\stackrel{(b)}{=} c_{n_{RX}, n_{RX}} S_{n_{RX}}^{\text{id}}(f) + c'_{n_{RX}, n'_{RX}} S_{n'_{RX}}^{\text{id}}(f), \quad (21)
 \end{aligned}$$

where at (a) we neglect the additional shift $\mu\Delta\tau$ of the sinc-function because of the limited bandwidth and small $\Delta\tau$. Furthermore, phase terms including the delay caused by coupling $\Delta\tau$ have been extracted and are shown to be constant for all measurements, as long as the previously made simplifications are justified. Therefore, at (b) these phase terms are included in the adapted coupling factor $c'_{n_{RX}, n'_{RX}} = c_{n_{RX}, n'_{RX}} e^{j\pi(2f_0 + \mu T)\Delta\tau}$, and the remaining signal parts correspond to the ideal signals of each channel as given by (11). Hence, it is shown that coupling effects can be approximated by a constant complex coupling factor for each pairwise antenna combination, thereby justifying the use of a coupling matrix \mathbf{C} such that

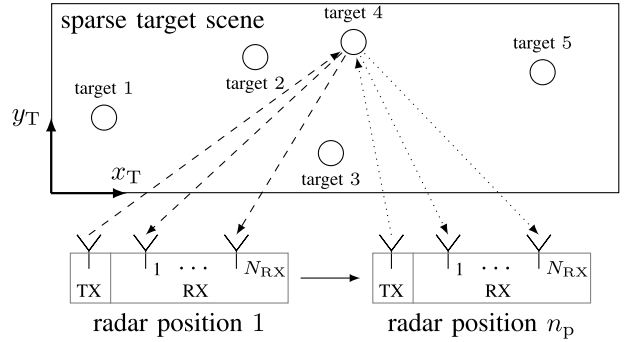


FIGURE 2. Exemplary illustration of the calibration process, assuming a moving radar and $N_T = 5$ targets forming a static scene.

$$S_{n_p}(f) = \mathbf{C} S_{n_p}^{\text{id}}(f), \quad (22)$$

with $S_{n_p}(f) = (S_{n_p, 1}^T(f), \dots, S_{n_p, N_{RX}}^T(f))^T$, and $S_{n_p}^{\text{id}}(f)$ formed equivalently.

Since (22) is valid for all frequency points f , it can also be applied to the discrete representation of the ideal signal in (17), resulting from the DFT. Because of the chosen order within the ideal measurement matrix \mathbf{H} as stacked matrices of (16), it is possible to apply the coupling matrix by using the Kronecker product, denoted by \otimes , such that the non-ideal measurement matrix including mutual coupling could be expressed as $\mathbf{H}_{\text{mc}} = \mathbf{C}_K \mathbf{H}$, with $\mathbf{C}_K = \mathbf{I}_{N_p N_{RX} N_s} \otimes \mathbf{C}$, and $\mathbf{I}_{N_p N_{RX} N_s}$ denoting the $N_p N_{RX} N_s \times N_p N_{RX} N_s$ identity matrix. The full radar measurement process including mutual coupling and complex channel dependent amplitudes can then be written using the ideal measurement matrix and a single matrix multiplication to include the non-idealities as

$$\mathbf{y} = \mathbf{C}_K \mathbf{H} \mathbf{x} + \mathbf{n}, \quad (23)$$

with the measured data $\mathbf{y} \in \mathbb{C}^{N_p N_{RX} N_s}$ in the frequency domain and uncorrelated additive white Gaussian noise (AWGN) with zero mean \mathbf{n} .

III. CALIBRATION APPROACH

In the following, the proposed calibration approach for estimating the unknown mutual coupling matrix \mathbf{C} is presented. First, the calibration setup is described and the main calibration idea is derived. Then, the algorithm is formulated as an iterative algorithm and possible problem relaxations for uniform linear arrays (ULA) are discussed. Finally, the approach is interpreted and compared to existing calibration procedures.

A. CALIBRATION BASED ON SPARSE SCENE

The mutual coupling calibration concept proposed in this work is based on measurements to a sparse scene, performed at different known relative positions, thereby creating a synthetic aperture. The basic calibration setup is shown in Fig. 2. The radar is positioned in front of an arbitrary and unknown sparse scene \mathbf{x} , which is rigid during the calibration process, i.e., the targets do not move relative to each other. Then, the

scene and radar are moved relatively to each other, i.e., either the radar or the target scene are moved to N_p known positions \mathbf{p}_{n_p} in a freely chosen reference frame, each time performing a single measurement. Note that no absolute positions of the targets or the radar have to be available. In the following, without loss of generality, we will assume a moving radar and a static scene.

In a controlled calibration setup using a man-made sparse scene, the type of targets, and therefore their scattering behavior, the number of targets N_T , as well as an estimate of their backscatter cross section A_{nT} , can be assumed to be known. For simplicity, we set $A_{nT} = A_T$, assuming all targets are of the same type. The measurement matrix in Section II was derived for point targets, which are generally assumed for radar imaging purposes. However, for known target types, the measurement matrix can be adapted to precisely describe the specific scattering behavior. This will exemplarily be shown in the measurement Section IV-A.

The measurement process can then be written as

$$\mathbf{y} = \mathbf{C}_K \mathbf{H}'(\mathbf{p}_1, \dots, \mathbf{p}_{N_T}) \mathbf{x}' + \mathbf{n}, \quad (24)$$

with the known target vector $\mathbf{x}' = (A_T, \dots, A_T)^T \in \mathbb{C}^{N_T}$ and the ideal measurement matrix \mathbf{H}' , which depends on the unknown positions \mathbf{p}_{nT} of the targets. To estimate the desired coupling matrix \mathbf{C} ,

$$\min_{\mathbf{C}, \mathbf{p}_1, \dots, \mathbf{p}_{N_T}} \|\mathbf{C}_K \mathbf{H}'(\mathbf{p}_1, \dots, \mathbf{p}_{N_T}) \mathbf{x}' - \mathbf{y}\|_2, \quad (25)$$

again with $\mathbf{C}_K = \mathbf{I}_{N_p N_{RX} N_s} \otimes \mathbf{C}$, has to be solved, but is non-convex. Therefore, for now, (25) is divided into two distinct optimizations.

B. CALIBRATION SUB-PROBLEMS

First, assuming known positions \mathbf{p}_{nT} , \mathbf{C} could directly be estimated via

$$\min_{\mathbf{C}} \|\mathbf{C}_K \mathbf{H}'(\mathbf{p}_1, \dots, \mathbf{p}_{N_T}) \mathbf{x}' - \mathbf{y}\|_2. \quad (26)$$

Second, assuming known coupling in (25) yields

$$\min_{\mathbf{p}_1, \dots, \mathbf{p}_{N_T}} \|\mathbf{C}_K \mathbf{H}'(\mathbf{p}_1, \dots, \mathbf{p}_{N_T}) \mathbf{x}' - \mathbf{y}\|_2. \quad (27)$$

Here, the measurement matrix depends nonlinearly on the positions $\mathbf{p}_1, \dots, \mathbf{p}_{N_T}$, which have to be estimated. Therefore, instead of estimating the target positions, an unknown target vector $\mathbf{x} \in \mathbb{C}^{N_x}$ containing target amplitudes at $N_x \gg N_T$ hypothetical known positions (x_T, y_T) can be estimated, yielding as an alternative problem with a linear dependency

$$\min_{\mathbf{x}} \|\mathbf{C}_K \mathbf{H} \mathbf{x} - \mathbf{y}\|_2 \text{ subject to } \|\mathbf{x}\|_0 = N_T, \quad (28)$$

assuming that the hypothetical positions include the true target positions. The measurement matrix \mathbf{H} can then be set up directly using the known hypothetical positions and is constant throughout the calibration process. Because this unconstrained problem is strongly under-determined, it has infinite solutions, as long as the target scene is sampled densely. Therefore, the constraint $\|\mathbf{x}\|_0 = N_T$, with the ℓ_0

pseudo-norm as the number of non-zero entries of \mathbf{x} , is added to limit the feasible set to target vectors \mathbf{x} with the correct number of targets. However, this constraint causes (28) to be NP-hard. Reviewing the measurement process, it is clear that the signal resulting from each single target can only be reconstructed optimally using one target at the correct position or multiple coherently superposing targets, which are located closely to the correct position. Hence, the signal of multiple targets with a sufficient distance can never be adequately reconstructed by using less hypothetical targets than actually present. Hence, the modified optimization problem of (28)

$$\min_{\mathbf{x}} \|\mathbf{C}_K \mathbf{H} \mathbf{x} - \mathbf{y}\|_2 \text{ subject to } \|\mathbf{x}\|_0 \leq N_T, \quad (29)$$

with a relaxed constraint $\|\mathbf{x}\|_0 \leq N_T$ will always be solved using $\|\mathbf{x}\|_0 = N_T$ targets.

To enable efficient solving of (29), now the ℓ_0 pseudo-norm is replaced by the ℓ_1 norm for convex relaxation, as it is typically done in compressed sensing [24], yielding

$$\min_{\mathbf{x}} \|\mathbf{C}_K \mathbf{H} \mathbf{x} - \mathbf{y}\|_2 \text{ subject to } \|\mathbf{x}\|_1 \leq k N_T A_T, \quad (30)$$

where the constraint is now bound to the expected total amplitude multiplied by an additional tuning parameter k . This type of constrained estimation in linear models is also called the *least absolute shrinkage and selection operator (lasso)* and was first introduced in [37]. The constraint enforces the selection of a sparse solution \mathbf{x} in (30). The tuning parameter is used to control the shrinkage of the estimates, thereby balancing the focus on a sparse solution in contrast to the least squares solution [37]. Under ideal conditions, in the proposed approach, k could be set to one. However, in real systems, multiple deviations from the ideal model occur. First, the chosen N_{TX} hypothetical target positions do not necessarily include the correct target positions. Second, the target amplitude A_T is only known as a rough estimate. Third, the matrix \mathbf{H} is only an approximate characterization of the measurement process. Effects of, e.g., the directional antenna characteristics are often not included, leading to amplitude variations of identical targets under different angles. Therefore, k should be chosen smaller than one, ensuring the shrinkage effect is strong enough for the desired sparse solution. In our experiments in Section IV, $k = 0.75$ was a good choice. Note that for $k < 1$ and a correctly assumed A_T the solution of (30) does not perfectly match with the solution of (29), because the targets' amplitudes are estimated too small.

C. COMBINED CALIBRATION

For the combined calibration, first, (26) is reformulated, so it incorporates the known target vector \mathbf{x} instead of the known target positions, thereby matching the formulation in (30). This yields the adapted problem

$$\min_{\mathbf{C}} \|\mathbf{C}_K \mathbf{H} \mathbf{x} - \mathbf{y}\|_2. \quad (31)$$

Now, because both distinct optimizations (30) and (31) are convex, the original problem (25) can be expressed as a biconvex problem and therefore be solved using an alternate convex search (ACS), as long as a prior estimate of either \mathbf{C} or \mathbf{x} is available [38].

However, in the combined optimization of (30) and (31), \mathbf{x} and \mathbf{C} can be arbitrarily scaled by inserting $\frac{1}{\alpha}\mathbf{x}$ and $\alpha\mathbf{C}$, yielding the same result in the objective functions. Thus, because of the intended shrinkage, caused by the constraint of (30), the target scene's amplitude will decrease, resulting in an increasing coupling matrix. Vice versa, the shrinkage behavior of (30) is affected and hence, \mathbf{x} becomes non-sparse, resulting in an inadequate calibration. Therefore, an additional constraint on the optimization parameters must be introduced to establish a constant ratio between the coupling's and the scene's size.

Because of coherent superposition of the targets, and an only approximately known value of A_T , the correct scaling is not straightforward. While multiple approaches are possible, we propose comparing the energy of the measured signal $E_y = \|\mathbf{y}\|_2^2$ with the sum of energies E_h resulting from N_T hypothetical sub-signals, such that

$$E_h = \sum_{n_T=1}^{N_T} \|(\mathbf{I}_{N_p N_{RX} N_s} \otimes \mathbf{C}) \mathbf{H}'(\mathbf{p}_{n_T}) A_T\|_2^2. \quad (32)$$

Here, the matrix $\mathbf{H}'(\mathbf{p}_{n_T})$ describes the measurement caused by a single target at the approximate target position \mathbf{p}_{n_T} , which is roughly estimated using the current estimate of \mathbf{x} . This approach implicitly assumes the radar's movement to be sufficiently large, so the average energy of the random coherent superpositions of the receive signals at different radar positions are a sufficiently good approximation for the expected receive energy.

From this energy comparison, a factor $\sqrt{E_y/E_h}$ can be derived to scale the coupling matrix or the amplitudes in \mathbf{x} . By performing the scaling operation, the estimation settles on one particular ratio between the target scene and the coupling matrix, which does not necessarily lead to the correctly scaled coupling matrix, but ensures the convergence of the algorithm while maintaining the restrictions made by the constraint in (30). Furthermore, it inherently compensates for errors made when assuming A_T to be known, by shifting this error into the scaling of \mathbf{C} or \mathbf{x} .

D. CALIBRATION ALGORITHM

The complete calibration algorithm is presented in Algorithm 1. First, the coupling matrix \mathbf{C}_0 is initialized as will be described in Section III-E. Furthermore, the signal energy E_y is calculated. Then, the ACS is performed in N_i iteration steps or until another termination criterion is reached.

During the i th step, \mathbf{x}_i and \mathbf{C}_i are estimated using (34b) and (34c). Then, the approximate N_T target positions $\mathbf{p}_{i,1}, \dots, \mathbf{p}_{i,N_T}$ are estimated in (34d), by, e.g., searching the

Algorithm 1 Mutual Coupling Calibration

1. Initialization:

$$i = 0 \quad (33a)$$

$$\mathbf{C}_0 = \text{get_initial_coupling_estimate} \quad (33b)$$

$$E_y = \|\mathbf{y}\|_2^2 \quad (33c)$$

2. Iteration:

while $i < N_i$ **do**

$$i = i + 1 \quad (34a)$$

$$\mathbf{x}_i = \underset{\mathbf{x}_i}{\operatorname{argmin}} \|(\mathbf{I}_{N_p N_{RX} N_s} \otimes \mathbf{C}_{i-1}) \mathbf{H} \mathbf{x}_i - \mathbf{y}\|_2 \quad (34b)$$

$$\text{subject to } \|\mathbf{x}_i\|_1 \leq k N_T A_T \quad (34b)$$

$$\mathbf{C}'_i = \underset{\mathbf{C}'_i}{\operatorname{argmin}} \|(\mathbf{I}_{N_p N_{RX} N_s} \otimes \mathbf{C}'_i) \mathbf{H} \mathbf{x}_i - \mathbf{y}\|_2 \quad (34c)$$

$$(\mathbf{p}_{i,1}, \dots, \mathbf{p}_{i,N_T}) = \text{estimate_positions}(\mathbf{x}_i) \quad (34d)$$

$$E_{h,i} = \sum_{n_T=1}^{N_T} \|(\mathbf{I}_{N_p N_{RX} N_s} \otimes \mathbf{C}'_i) \mathbf{H}'(\mathbf{p}_{i,n_T}) A_T\|_2^2 \quad (34e)$$

$$\mathbf{C}_i = \sqrt{\frac{E_y}{E_{h,i}}} \mathbf{C}'_i \quad (34f)$$

end while

N_T highest values in \mathbf{x}_i and choosing the corresponding hypothetical positions. These are then used in (34e) to calculate the summed hypothetical energy $E_{h,i}$ and scale the coupling matrix accordingly in (34f). Alternatively, \mathbf{x}_i can be scaled between (34b) and (34c). In this case, however, A_T would have to be scaled as well.

E. INITIAL ESTIMATION OF THE COUPLING MATRIX

The biconvex problem of simultaneously estimating the coupling matrix and an unknown sparse scene can only be solved locally based on an initial estimation of one of the desired parameters. For this purpose, many approaches are possible, such as creating an image of the scenery using a single antenna, which does not require calibration. However, this requires a sufficiently long synthetic aperture to estimate \mathbf{x}_0 reliably. Therefore, we propose to initially estimate the coupling matrix \mathbf{C}_0 , again utilizing the scene's sparsity. For this prior estimate both coupling effects and amplitude factors at each channel are neglected, thereby reducing the unknowns to $N_{RX} - 1$ phase values $\varphi_{n_{RX}}$ on the main diagonal of \mathbf{C}_0 , while setting one arbitrary channel, here channel N_{RX} , as a reference for the phase. Furthermore, when neglecting coupling, each channel's phase-offset can be calibrated individually, relative to the reference channel. This can be achieved by solving a non-convex problem with a convex optimization similar to a reduced version of (30) as the objective

$$\begin{aligned} & \min_{\varphi_{n_{RX}}} \min_{\mathbf{x}} \|(\mathbf{I}_{N_p N_{RX} N_s} \otimes \mathbf{C}_{0,n_{RX}}) \mathbf{H}_{n_{RX}} \mathbf{x} - \mathbf{y}_{n_{RX}}\|_2 \\ & \text{subject to } \|\mathbf{x}\|_1 \leq N_T A_T, \end{aligned} \quad (35)$$

with the reduced diagonal coupling matrix

$$\mathbf{C}_{0,n_{RX}} = \begin{pmatrix} 1 & 0 \\ 0 & e^{j\varphi_{n_{RX}}} \end{pmatrix} \quad (36)$$

and $\mathbf{H}_{n_{RX}}$ and $\mathbf{y}_{n_{RX}}$ as the reduced measurement matrix and vector, containing only the relevant rows for channels n_{RX} and N_{RX} . Equation (35) can now be solved, with reasonable computational effort, by a global search over $\varphi_{n_{RX}}$ in the value range $[-\pi, \pi]$.

F. INTERPRETATION AND COMPARISON

The calibration of measurement systems is commonly based on the evaluation of reference measurements with a known expected result to estimate the unknown calibration parameters. In radar systems, the reference measurements require targets at precisely known positions relative to the radar, i.e., known within the order of the fraction of a wavelength of the carrier frequency. This causes extremely high requirements for a reference system, which can hardly be met in practice. Therefore, in common approaches these requirements are lowered by performing far-field measurements to targets under different known angles in specific environments such as an anechoic chamber. However, these measurements have to be processed incoherently, because the true relative distances are not known, yielding unknown phase and amplitude factors for every measurement to a different angle. Therefore, the effective information gain of each measurement is limited.

In the proposed calibration approach, the target positions are estimated relative to the radar as part of the calibration process itself. Thereby the high requirements on the reference system are reduced significantly, because only the relative movement of the radar must be known precisely. The measurements performed at the different radar positions can be processed coherently to form a synthetic aperture, because the passive target scene is constant during the complete measurement process. Therefore, the information about the target scene is contained in the measurements creating a synthetic aperture of each separate RX channel, without requiring any calibration data. Consequently, the relative information between the channels, i.e., amplitude and phase factors, and mutual coupling, can be extracted knowing that all channels measure to the same target scene. The underdeterminedness of this problem, already reduced by the usage of the synthetic aperture, is further decreased by exploiting the knowledge of a sparse target scene, a process which is commonly known from compressed sensing [23], [24].

In contrast to common approaches using known angles, where with each incoherent measurement an additional complex amplitude has to be estimated, the coherent evaluation of measurements to a static scene via a synthetic aperture reduces the number of additional unknown parameters to effectively one position per target for the complete calibration process. Therefore, the number of unknowns is independent from the number of measurements and the full information contained in the measurements can be exploited.

Generally, during calibration measurements, no correlated errors such as crosstalk and multipaths should occur, hence, standard calibration procedures requiring far-field conditions are performed in anechoic chambers. In this approach, which does not make far-field assumptions, multipath can easily be avoided by placing the target scene close to the sensor and with sufficient distance to any strong reflectors such as the floor or ceiling. Then, assuming commonly used FMCW radar systems with a sufficiently high bandwidth, the delay of the desired line-of-sight (LOS) and the multipath can be easily separated in the frequency domain signal, where each frequency bin corresponds to a certain delay and target distance. Because the approximate distance between the targets and the radar is known, the evaluated frequency components can be limited to the expected range. Thereby, signal components containing crosstalk and multipath are discarded. Furthermore, because the target scene is located in the near-field of the synthetic aperture, possibly remaining multipath components change over the aperture and can therefore be approximated as uncorrelated noise [14].

G. PROBLEM RELAXATION FOR UNIFORM LINEAR ARRAYS

Uniform linear arrays (ULA) are often used in standard MIMO radar sensors, especially in automotive applications, because they enable very efficient signal processing [35], [39]. However, in a single measurement to a target located in the far-field of the physical array aperture, an ULA produces redundant information between antenna pairs with the same spacing. Because coupling mainly depends on the antenna distance, measurements from one antenna pair can be partially explained using the signals of another antenna pair with identical spacing, which yield the same phase difference. This effect is reduced for larger apertures resulting from the radar movement, because the targets are then in the effective near-field of the full aperture. Nevertheless, it is favorable and a common simplification to reduce the number of parameters in \mathbf{C} by exploiting the array structure [8], [22], [31]. For this purpose, it is assumed that at first the signal couples between the antennas, described by the matrix \mathbf{Z} . For ULAs it is common to assume \mathbf{Z} to be a symmetric Toeplitz matrix with ones on the main diagonal, i.e., to assign a common coupling coefficient for all antenna pairs with identical spacing [22], [40]. Then, at each channel the signal is multiplied with a complex gain using the matrix $\boldsymbol{\Gamma}$, describing the channel mismatches. This yields the overall coupling matrix $\mathbf{C} = \boldsymbol{\Gamma}\mathbf{Z}$.

To estimate these matrices separately, the calibration process must be split up further, again using ACS. The complete procedure is described in Algorithm 2. \mathbf{C}_i in Algorithm 1 is replaced by $\boldsymbol{\Gamma}_i\mathbf{Z}_i$; \mathbf{Z}_0 is initialized as a identity matrix and $\boldsymbol{\Gamma}_0$ is initialized similarly to (33b). Equation (34c) is replaced by an iterative estimation of $\boldsymbol{\Gamma}$ and \mathbf{Z} . The scaling operation is then applied to the complex amplitudes $\boldsymbol{\Gamma}_i$.

Algorithm 2 Mutual Coupling Calibration for ULAs

1. Initialization:

$$i = 0 \quad (37a)$$

$$\boldsymbol{\Gamma}_0 = \text{get_initial_coupling_estimate} \quad (37b)$$

$$\mathbf{Z}_0 = \mathbf{I}_{N_{\text{RX}}} \quad (37c)$$

$$E_y = \|\mathbf{y}\|_2^2 \quad (37d)$$

2. Iteration of the full calibration:

while $i < N_i$ **do**

$$i = i + 1 \quad (38a)$$

$$\mathbf{x}_i = \underset{\mathbf{x}_i}{\text{argmin}} \|(\mathbf{I}_{N_p N_{\text{RX}} N_s} \otimes (\boldsymbol{\Gamma}_{i-1} \mathbf{Z}_{i-1})) \mathbf{H} \mathbf{x}_i - \mathbf{y}\|_2 \quad (38b)$$

$$\text{subject to } \|\mathbf{x}_i\|_1 \leq N_{\text{TAT}} \quad (38b)$$

3. Estimating the coupling matrix

3.1 Initialization of the coupling estimation:

$$j = 0 \quad (39a)$$

$$\boldsymbol{\Gamma}_i^0 = \boldsymbol{\Gamma}_{i-1} \quad (39b)$$

$$\mathbf{Z}_i^0 = \mathbf{Z}_{i-1} \quad (39c)$$

3.2 Iteration of the coupling estimation:

while $j < N_j$ **do**

$$j = j + 1 \quad (40a)$$

$$\text{subject to } \|\mathbf{x}_i\|_1 \leq N_{\text{TAT}}$$

$$\boldsymbol{\Gamma}_i^j \text{ is diagonal} \quad (40b)$$

$$\mathbf{Z}_i^j = \underset{\mathbf{Z}_i^j}{\text{argmin}} \|(\mathbf{I}_{N_p N_{\text{RX}} N_s} \otimes (\boldsymbol{\Gamma}_i^j \mathbf{Z}_i^j)) \mathbf{H} \mathbf{x}_i - \mathbf{y}\|_2 \quad (40c)$$

$$\text{subject to } \|\mathbf{x}_i\|_1 \leq N_{\text{TAT}}$$

$$\mathbf{Z}_i^j \text{ is symmetric and Toeplitz} \quad (40c)$$

end while

3.3 Assignment and scaling:

$$\boldsymbol{\Gamma}'_i = \boldsymbol{\Gamma}_i^{N_j} \quad (41a)$$

$$\mathbf{Z}_i = \mathbf{Z}_i^{N_j} \quad (41b)$$

$$(\mathbf{p}_{i,1}, \dots, \mathbf{p}_{i,N_{\text{T}}}) = \text{estimate_positions}(\mathbf{x}_i) \quad (42a)$$

$$E_{\text{h},i} = \sum_{n_{\text{T}}=1}^{N_{\text{T}}} \|(\mathbf{I}_{N_p N_{\text{RX}} N_s} \otimes (\boldsymbol{\Gamma}'_i \mathbf{Z}_i')) \mathbf{H}' (\mathbf{p}_{i,n_{\text{T}}}) A_{\text{T}}\|_2^2 \quad (42b)$$

$$\boldsymbol{\Gamma}_i = \sqrt{\frac{E_y}{E_{\text{h},i}}} \boldsymbol{\Gamma}'_i \quad (42c)$$

end while

IV. MEASUREMENT

To validate the proposed calibration procedure, a real-life radar calibration was performed. In this section, first, the measurement setup will be described. Then, the estimated

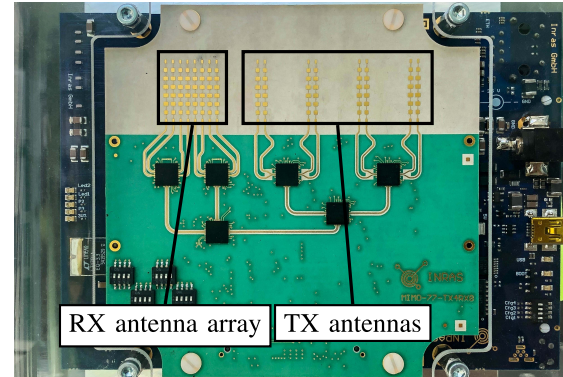


FIGURE 3. MIMO radar used for the measurement, comprising $N_{\text{RX}} = 8$ RX antennas and 4 TX antennas.

coupling behavior is shown and verified by comparing imaging results using the proposed calibration and the manufacturer's calibration.

A. MEASUREMENT SETUP

The used radar system is a commercially available FMCW MIMO radar system from INRAS with a front-end operating at the frequency $f_0 = 77$ GHz with a bandwidth of $B = 1$ GHz, which is depicted in Fig. 3. The front-end comprises $N_{\text{RX}} = 8$ receive antennas, arranged as a ULA, and 4 transmit antennas, whereas only a single transmit antenna is considered for the calibration. The MIMO radar calibration data given in the product data sheet serves as a reference for the proposed calibration. According to the data sheet, this standard calibration data was achieved by measuring to a corner reflector at an angle of 0° in an anechoic chamber, i.e., by a conventional calibration procedure. Only the complex amplitudes per channel were calibrated, neglecting mutual coupling.

The proposed calibration is performed indoors in the entrance area of an office building, with the radar mounted on a linear unit with a step motor providing a relative position reference for the radar, while enabling a maximal synthetic aperture of 0.75 m. The complete setup is shown in Fig. 4. Six metal spheres with a radius $r = 4$ cm serve as targets. The measurement matrix is adapted to fit the scattering behavior of the spheres, by changing (4) to

$$\tau_{n_{\text{p}}, n_{\text{RX}}, n_{\text{T}}} \approx \frac{d_{\text{TX} \rightarrow n_{\text{T}}, n_{\text{p}}} + d_{n_{\text{T}} \rightarrow n_{\text{RX}}, n_{\text{p}}} - 2r + d_{\text{off}}}{c_0}, \quad (43)$$

which is a justified approximation for small r and if the TX antenna is located close to the receivers. Both is valid in this case. Furthermore, a distance offset $d_{\text{off}} = 11.5$ cm was introduced, which compensates for additional signal delays within the radar's hardware and was determined using a simple distance pre-calibration.

To avoid multipath, the spheres and the radar were located approximately half way between the floor and ceiling, without strong reflecting objects in the area of the spheres. For this purpose, the spheres are placed at random positions

with a distance of 1.5 to 2.5 m from the radar on a structure made from extruded polystyrene rigid foam, which is known to have a dielectric constant close to 1 and almost no transmission losses at the radar frequency around 77 GHz. It can therefore be assumed invisible to the radar system. The radar on the linear unit is positioned at approximately the same height as the targets. For the antenna array calibration, measurements were performed at $N_p = 30$ positions within the 0.75 m aperture, available by the linear unit.

B. CALIBRATION RESULTS

The MIMO radar's receive antenna array is a ULA, therefore, the problem relaxation proposed in Section III-G was used for the calibration process. The shrinkage design parameter was chosen as $k = 0.75$. The estimated absolute values of the diagonal gain matrix, normed to the first entry, are

$$|\boldsymbol{\Gamma}| = \text{diag}(1.00, 1.11, 0.95, 0.98, 0.87, 1.13, 1.09, 1.13), \quad (44)$$

and of the coupling matrix

$$|\mathbf{Z}| = \begin{pmatrix} 1.00 & 0.12 & 0.07 & 0.06 & 0.05 & 0.01 & 0.03 & 0.02 \\ 0.12 & 1.00 & 0.12 & 0.07 & 0.06 & 0.05 & 0.01 & 0.03 \\ 0.07 & 0.12 & 1.00 & 0.12 & 0.07 & 0.06 & 0.05 & 0.01 \\ 0.06 & 0.07 & 0.12 & 1.00 & 0.12 & 0.07 & 0.06 & 0.05 \\ 0.05 & 0.06 & 0.07 & 0.12 & 1.00 & 0.12 & 0.07 & 0.06 \\ 0.01 & 0.05 & 0.06 & 0.07 & 0.12 & 1.00 & 0.12 & 0.07 \\ 0.03 & 0.01 & 0.05 & 0.06 & 0.07 & 0.12 & 1.00 & 0.12 \\ 0.02 & 0.03 & 0.01 & 0.05 & 0.06 & 0.07 & 0.12 & 1.00 \end{pmatrix}. \quad (45)$$

As expected, $|\mathbf{Z}|$ is dominated by the main diagonal, and the coupling strength degrades with increasing antenna distance. Only coefficients in the outer corner of the matrix, describing the coupling of RX antennas with large distances, increase slightly. This indicates further small coupling effects, which go beyond the assumption of coupling resulting solely from reflections at the antennas, such as coupling within the hardware or between the TX antennas. Furthermore, small errors in the modeling of the measurement matrix may cause deviations of the numerical estimate from the correct matrix. Unfortunately, no correct coupling matrix could be measured for reference.

C. IMAGING RESULTS

To further validate the proposed calibration, additional measurements using a similar setup as shown in Fig. 4 were performed to single metal spheres at different positions \mathbf{p}_T . The target's positions can be expressed in polar coordinates, i.e., an angle θ_T and a distance d_T with respect to the radar's first measurement position. The targets' positions did not coincide with the target positions used for calibration. At each angle, data was collected from 13 radar positions and combined to a total synthetic aperture of $d_{sa} = 11.4$ cm. Then, radar images with the image amplitudes $|\mathbf{S}|$ were reconstructed by standard matched filtering [34] using the

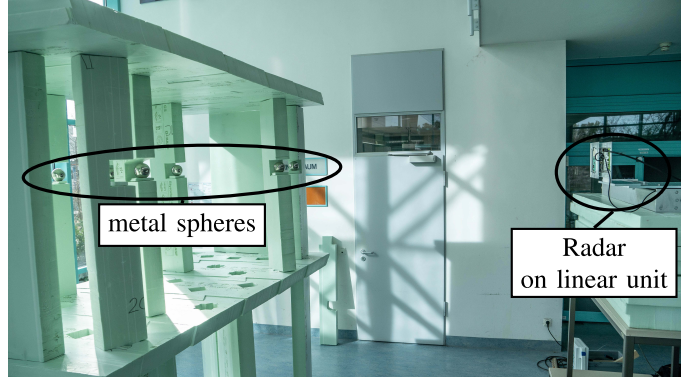


FIGURE 4. Indoor calibration setup comprising six metal spheres positioned randomly on a structure made of extruded polystyrene rigid foam. The MIMO radar is mounted on a linear unit.

estimated calibration data and the standard calibration data for reference. The radar images for three target angles θ_T of approximately 0° , 24° , and 34° , are shown in Fig. 5.

The imaging performance is evaluated based on different measures. First, the mainlobe magnitude (MLM), normed to the MLM at 0° , serves as a measure for the correct coherent superposition of the target. Second, the sidelobe level (SLL) as the distance of the first and thereby highest sidelobe magnitude to the MLM, which mainly results from the limited aperture and the underlying point spread function, are an additional measure for the achieved focusing. Third, the spurious free dynamic range (SFDR) is defined as the distance of the highest spurious signal's magnitude to the MLM. A peak is considered a spurious signal instead of a sidelobe if it is located more than 1.5 times the angular resolution δ_θ , as given by the Rayleigh criterion [36] $\delta_\theta = 1.22 \frac{f_0}{c_0 d_{sa}}$, away from the mainlobe peak. For the system at hand and the given synthetic aperture size this yields an angular boundary of $1.5 \delta_\theta = 3.7^\circ$.

For the evaluation, the MLM, the magnitude of the highest sidelobe, and the resulting SLL are marked in the reconstructed images in Fig. 5. All images show a clearly reconstructed target with low sidelobes, demonstrating that the proposed calibration procedure leads to a valid coupling matrix, which can be used for imaging purposes. Nevertheless, the MLM decreases with increasing target angles using both calibrations, although all targets have an identical cross section. Because of the antennas' directional characteristics, a certain reduction of the MLM is expected for larger angles. Furthermore, the target distance differs slightly, causing additional variations. However, the MLM of the targets at 24° and 34° are significantly higher when using the proposed calibration, hence showing a noticeably improved coherent superposition for larger angles when compared to the ex-factory calibration. The SLL only varies little over the angles and different calibrations. At 0° , the standard calibration yields a slightly higher SLL, whereas the proposed calibration yields an improved SLL at larger angles.

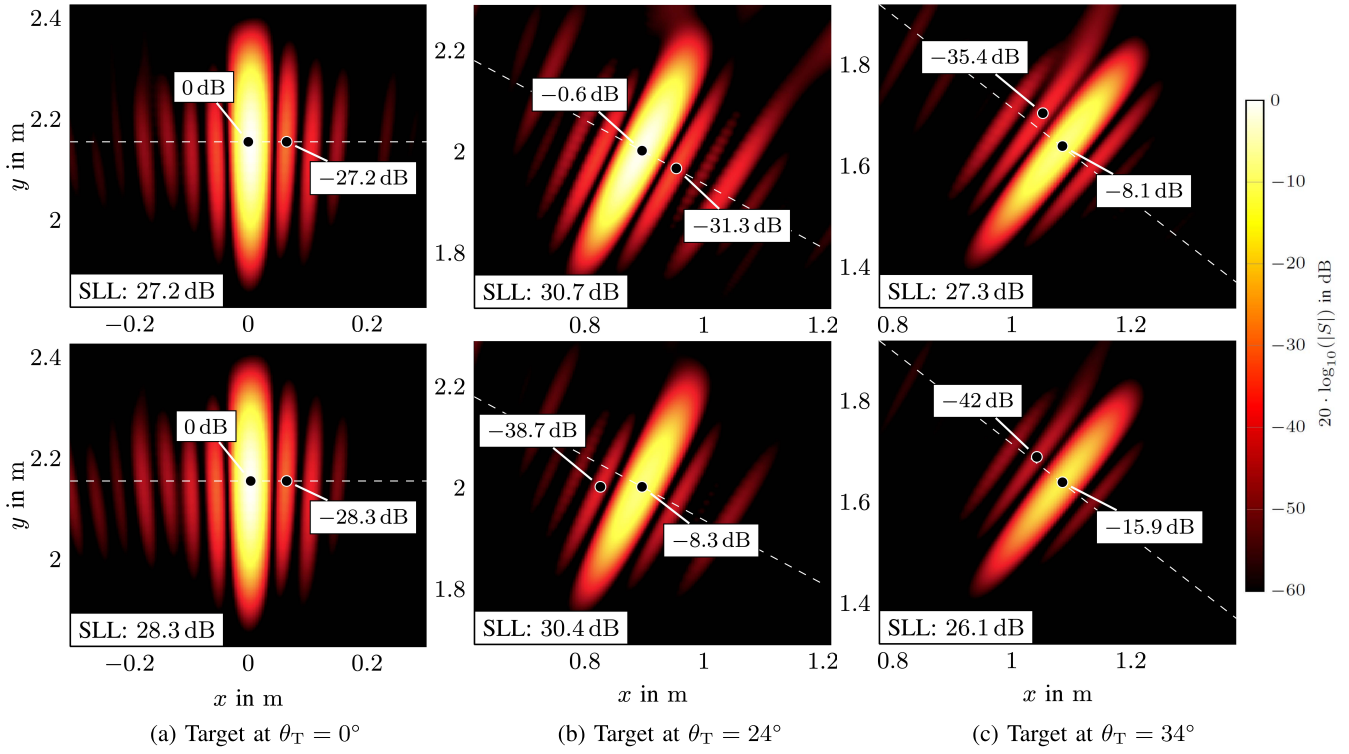


FIGURE 5. Image reconstructions of single targets under different angles θ_T , for each angle reconstructed using the data from the proposed calibration (top) and the standard calibration data (bottom) for reference.

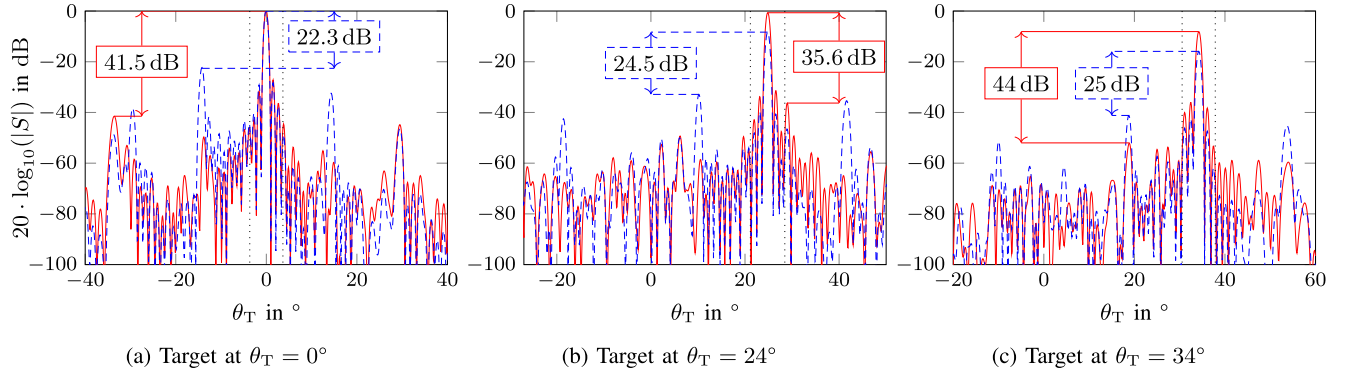


FIGURE 6. Profiles of the reconstructed image amplitudes $|S|$ at the true target distance over hypothetical target angles θ_T as indicated by the white dashed lines in Fig. 5, for the standard (dashed blue) and the proposed calibration (red), with the respective SFDR. The angular boundary $1.5 \delta_\theta = 3.7^\circ$ for spurious signals is indicated by dotted lines.

These performance differences can be explained reviewing that a single target at 0° was used for the standard calibration data, which incorporates coupling effects within the complex gains, yielding an optimized result at this angle, but leads to degraded performance at other angles. In the proposed approach, targets at multiple angles were used, enabling the separate estimation of complex gains and coupling, thereby yielding a calibration matrix which is optimized for a more evenly performance over a larger angle area.

To evaluate the SFDR of the radar images, we consider the profiles of the reconstructed image amplitudes $|S|$ at the true target distance d_T , i.e., through the mainlobe, as indicated by the white dashed lines in Fig. 5 over a larger area

of hypothetical target angles. These profiles are shown in Fig. 6 for both calibrations and the different targets, with the marked SFDR and the previously defined boundaries for the spur definition as dotted lines. When using the standard calibration data, strong spurious signals occur, yielding a SFDR smaller than the SLL and showing systematic errors in the reconstruction caused by mutual coupling, which may lead to the false detection of ghost targets. When using the proposed calibration, which includes coupling and therefore reduces the amount of systematic errors, the SFDR is increased significantly by 10 to 19 dB, thereby improving the image quality and strongly reducing the risk of detecting unwanted ghost targets. Especially in more complex imaging

scenarios, this suppression of spurious signals is important to correctly distinguish small targets from ghost targets under large angles. For example, in Fig. 6 the magnitude distance of the spurious signal resulting from the target at 0° to the true target's amplitude at 34° is increased from 6 dB to 33.4 dB when using the proposed calibration.

Overall, the novel calibration procedure outperforms the manufacturer's calibration, which only includes complex gains. It yields significantly improved imaging results with increased main lobes and simultaneously decreased spurious signals, whereas the calibration's hardware effort was reduced drastically. The calibration performance of standard procedures can be increased compared to the ex-factory calibration by estimating coupling via measuring to a large number of targets under different angles, as it is done, e.g., in [12]. However, this would further increase the requirements on the calibration hardware and procedure. This shows the advantage of our approach, which was performed indoors, without taking strong effort to suppress multipath propagation or requiring precise target positions, hence, in an environment, in which common calibration approaches would fail.

V. CONCLUSION

In this paper, a novel mutual coupling calibration procedure was presented, which uses a synthetic aperture and sparsely distributed targets at unknown locations in the array's near-field. In the approach, the target scene is reconstructed simultaneously with the coupling matrix estimation. Thereby, it overcomes the limitations of standard approaches, which are usually performed cumbersomely in anechoic chambers providing a multipath free far-field environment. The approach was successfully validated by measurements with low hardware requirements in an indoor environment, outperforming the used radar's ex-factory calibration, which did not consider mutual coupling. Because the synthetic aperture can be either created by moving the radar or the target scene, this procedure is also suited for quick in-situ calibration with low effort of, e.g., automotive radar sensors. To further increase the calibration performance and efficiency, the antennas' directional characteristics can be incorporated into the measurement model. Furthermore, the same procedure can be used to calibrate other radar parameters such as antenna phase centers. Finally, it should be noted that while the hardware effort of the proposed calibration has been reduced, the computational effort has increased. Therefore, the necessary computing power should be reduced for an industrial application.

ACKNOWLEDGMENT

The authors would like to thank Lea Egermann and Laura Ervin for their time, effort, and creativity while creating the extruded polystyrene measurement setup.

REFERENCES

- [1] J. Dickmann *et al.*, "Automotive radar—the key technology for autonomous driving: From detection and ranging to environmental understanding," in *Proc. IEEE Radar Conf.*, May 2016, pp. 1–6.
- [2] J. Geiß, E. Sippel, P. Gröschel, M. Hehn, M. Schütz, and M. Vossiek, "A wireless local positioning system concept and 6D localization approach for cooperative robot swarms based on distance and angle measurements," *IEEE Access*, vol. 8, pp. 115501–115514, 2020.
- [3] I. Immoreev and T.-H. Tao, "UWB radar for patient monitoring," *IEEE Aerosp. Electron. Syst. Mag.*, vol. 23, no. 11, pp. 11–18, Nov. 2008.
- [4] S. S. Ahmed, A. Schiessl, F. Gumbmann, M. Tiebout, S. Methfessel, and L.-P. Schmidt, "Advanced microwave imaging," *IEEE Microw. Mag.*, vol. 13, no. 6, pp. 26–43, Sep./Oct. 2012.
- [5] W. L. Melvin, "A STAP overview," *IEEE Aerosp. Electron. Syst. Mag.*, vol. 19, no. 1, pp. 19–35, Jan. 2004.
- [6] N. Ö. Onhon and M. Cetin, "A sparsity-driven approach for joint SAR imaging and phase error correction," *IEEE Trans. Image Process.*, vol. 21, no. 4, pp. 2075–2088, Apr. 2012.
- [7] E. Fishler, A. Haimovich, R. Blum, D. Chizhik, L. Cimini, and R. Valenzuela, "MIMO radar: An idea whose time has come," in *Proc. IEEE Radar Conf.*, 2004, pp. 71–78.
- [8] M. Viberg, M. Lanne, and A. Lundgren, "Calibration in array processing," in *Classical and Modern Direction-of-Arrival Estimation*. Burlington, MA, USA: Elsevier, 2009, pp. 93–124.
- [9] I. Gupta and A. Ksieniak, "Effect of mutual coupling on the performance of adaptive arrays," *IEEE Trans. Antennas Propag.*, vol. 31, no. 5, pp. 785–791, Sep. 1983.
- [10] C. M. Schmid, S. Schuster, R. Feger, and A. Stelzer, "On the effects of calibration errors and mutual coupling on the beam pattern of an antenna array," *IEEE Trans. Antennas Propag.*, vol. 61, no. 8, pp. 4063–4072, Aug. 2013.
- [11] B. Porat and B. Friedlander, "Accuracy requirements in off-line array calibration," *IEEE Trans. Aerosp. Electron. Syst.*, vol. 33, no. 2, pp. 545–556, Apr. 1997.
- [12] C. M. Schmid, C. Pfeffer, R. Feger, and A. Stelzer, "An FMCW MIMO radar calibration and mutual coupling compensation approach," in *Proc. Eur. Radar Conf.*, Oct. 2013, pp. 13–16.
- [13] B. C. Ng and C. M. S. See, "Sensor-array calibration using a maximum-likelihood approach," *IEEE Trans. Antennas Propag.*, vol. 44, no. 6, pp. 827–835, Jun. 1996.
- [14] E. Sippel, M. Lipka, J. Geiß, M. Hehn, and M. Vossiek, "In-situ calibration of antenna arrays within wireless locating systems," *IEEE Trans. Antennas Propag.*, vol. 68, no. 4, pp. 2832–2841, Apr. 2020.
- [15] C. Vasanelli *et al.*, "Calibration and direction-of-arrival estimation of millimeter-wave radars: A practical introduction," *IEEE Antennas Propag. Mag.*, vol. 62, no. 6, pp. 34–45, Dec. 2020.
- [16] A. J. Weiss and B. Friedlander, "Array shape calibration using sources in unknown locations—a maximum likelihood approach," *IEEE Trans. Acoust., Speech, Signal Process.*, vol. 37, no. 12, pp. 1958–1966, Dec. 1989.
- [17] A. Paulraj and T. Kailath, "Direction of arrival estimation by eigenstructure methods with unknown sensor gain and phase," in *Proc. IEEE Int. Conf. Acoust. Speech Signal Process.*, vol. 10, Apr. 1985, pp. 640–643.
- [18] P. Gröschel *et al.*, "A system concept for online calibration of massive MIMO transceiver arrays for communication and localization," *IEEE Trans. Microw. Theory Techn.*, vol. 65, no. 5, pp. 1735–1750, May 2017.
- [19] Y. Rockah and P. Schultheiss, "Array shape calibration using sources in unknown locations—Part I: Far-field sources," *IEEE Trans. Acoust., Speech, Signal Process.*, vol. 35, no. 3, pp. 286–299, Mar. 1987.
- [20] Y. Rockah and P. Schultheiss, "Array shape calibration using sources in unknown locations—Part II: Near-field sources and estimator implementation," *IEEE Trans. Acoust., Speech, Signal Process.*, vol. 35, no. 6, pp. 724–735, Jun. 1987.
- [21] F. Sellone and A. Serra, "A novel online mutual coupling compensation algorithm for uniform and linear arrays," *IEEE Trans. Signal Process.*, vol. 55, no. 2, pp. 560–573, Feb. 2007.
- [22] B. Friedlander and A. J. Weiss, "Direction finding in the presence of mutual coupling," *IEEE Trans. Antennas Propag.*, vol. 39, no. 3, pp. 273–284, Mar. 1991.
- [23] D. L. Donoho, "Compressed sensing," *IEEE Trans. Inf. Theory*, vol. 52, no. 4, pp. 1289–1306, Apr. 2006.
- [24] E. Candes, J. Romberg, and T. Tao, "Robust uncertainty principles: Exact signal reconstruction from highly incomplete frequency information," *IEEE Trans. Inf. Theory*, vol. 52, no. 2, pp. 489–509, Feb. 2006.

- [25] J. H. Ender, "On compressive sensing applied to radar," *Signal Process.*, vol. 90, no. 5, pp. 1402–1414, May 2010.
- [26] M. A. Herman and T. Strohmer, "High-resolution radar via compressed sensing," *IEEE Trans. Signal Process.*, vol. 57, no. 6, pp. 2275–2284, Jun. 2009.
- [27] S. Ling and T. Strohmer, "Self-calibration and biconvex compressive sensing," *Inverse Problems*, vol. 31, no. 11, Nov. 2015, Art. no. 115002.
- [28] Ç. Bilen, G. Puy, R. Gribonval, and L. Daudet, "Convex optimization approaches for blind sensor calibration using sparsity," *IEEE Trans. Signal Process.*, vol. 62, no. 18, pp. 4847–4856, Sep. 2014.
- [29] S. J. Wijndholds and S. Chiarucci, "Blind calibration of phased arrays using sparsity constraints on the signal model," in *Proc. 24th Eur. Signal Process. Conf. (EUSIPCO)*, Aug. 2016, pp. 270–274.
- [30] A. M. Elbir and T. E. Tuncer, "Sparse support recovery for DOA estimation in the presence of mutual coupling," in *Proc. 23rd Eur. Signal Process. Conf. (EUSIPCO)*, Aug. 2015, pp. 1366–1370.
- [31] A. M. Elbir and T. E. Tuncer, "2-D DOA and mutual coupling coefficient estimation for arbitrary array structures with single and multiple snapshots," *Digit. Signal Process.*, vol. 54, pp. 75–86, Jul. 2016.
- [32] M. Murad *et al.*, "Requirements for next generation automotive radars," in *Proc. IEEE Radar Conf. (RadarCon)*, Apr. 2013, pp. 1–6.
- [33] C. Shipley and D. Woods, "Mutual coupling-based calibration of phased array antennas," in *Proc. IEEE Int. Conf. Phased Array Syst. Technol.*, May 2000, pp. 529–532.
- [34] J. C. Curlander and R. N. McDonough, *Synthetic Aperture Radar*, vol. 11. New York, NY, USA: Wiley, 1991.
- [35] S. M. Patole, M. Torlak, D. Wang, and M. Ali, "Automotive radars: A review of signal processing techniques," *IEEE Signal Process. Mag.*, vol. 34, no. 2, pp. 22–35, Mar. 2017.
- [36] J. Hasch, E. Topak, R. Schnabel, T. Zwick, R. Weigel, and C. Waldschmidt, "Millimeter-wave technology for automotive radar sensors in the 77 GHz frequency band," *IEEE Trans. Microw. Theory Techn.*, vol. 60, no. 3, pp. 845–860, Mar. 2012.
- [37] R. Tibshirani, "Regression shrinkage and selection via the Lasso," *J. Royal Statist. Soc. B, Methodol.*, vol. 58, no. 1, pp. 267–288, Jan. 1996.
- [38] J. Gorski, F. Pfeuffer, and K. Klamroth, "Biconvex sets and optimization with biconvex functions: A survey and extensions," *Math. Methods Oper. Res.*, vol. 66, no. 3, pp. 373–407, Jun. 2007.
- [39] F. Engels, P. Heidenreich, A. M. Zoubir, F. K. Jondral, and M. Wintermantel, "Advances in automotive radar: A framework on computationally efficient high-resolution frequency estimation," *IEEE Signal Process. Mag.*, vol. 34, no. 2, pp. 36–46, Mar. 2017.
- [40] T. Svantesson, "Modeling and estimation of mutual coupling in a uniform linear array of dipoles," in *Proc. IEEE Int. Conf. Acoust. Speech Signal Process.*, vol. 5, Mar. 1999, pp. 2961–2964.



JOHANNA GEISS (Graduate Student Member, IEEE) was born in Lich, Germany, in 1992. She received the master's degree in electrical engineering from Friedrich-Alexander-Universität Erlangen-Nürnberg, Erlangen, Germany, in 2017, where she is currently pursuing the Ph.D. degree with the Institute of Microwaves and Photonics (LHFT). She is primarily working in the fields of radar-based localization, sensor-fusion, radar signal processing, radar calibration, and ego-motion estimation.



ERIK SIPPEL was born in Fürth, Germany, in 1991. He received the M.Sc. degree in electronic engineering from Friedrich-Alexander-Universität Erlangen-Nürnberg (FAU), Erlangen, Germany, in 2015, where he is currently pursuing the Ph.D. degree.

In 2016, he joined the Institute of Microwaves and Photonics, FAU. His current research interests include indoor localization, especially radar for near-field localization, data transmission, and analog-to-digital conversion.



MARKUS HEHN (Graduate Student Member, IEEE) was born in Bamberg, Germany, in 1987. He received the M.Sc. degree in electrical engineering from Friedrich-Alexander-Universität Erlangen-Nürnberg (FAU), Erlangen, Germany, in 2016, where he is currently pursuing the Ph.D. degree.

In 2016, he joined the Institute of Microwaves and Photonics, FAU. His current research interests include radar for near-field localization and localization systems for indoor environment.



MARTIN VOSSIEK (Fellow, IEEE) received the Ph.D. degree from Ruhr-Universität Bochum, Bochum, Germany, in 1996. In 1996, he joined Siemens Corporate Technology, Munich, Germany, where he was the Head of the Microwave Systems Group from 2000 to 2003. Since 2003, he has been a Full Professor with Clausthal University, Clausthal-Zellerfeld, Germany. Since 2011, he has been the Chair of the Institute of Microwaves and Photonics (LHFT), Friedrich-Alexander Universität Erlangen-Nürnberg, Erlangen, Germany. He has authored or coauthored more than 250 articles. His research has led to over 90 granted patents. His current research interests include radar, transponder, RF identification, communication, and locating systems. He was a recipient of several international awards. For example, recently, he was awarded the 2019 Microwave Application Award from the IEEE Microwave Theory and Techniques Society (MTT-S). He was the Founding Chair of the MTT IEEE Technical Coordinating Subcommittee MTT-27 Wireless-Enabled Automotive and Vehicular Application. He has served on the Review Boards for numerous technical journals. From 2013 to 2019, he was an Associate Editor for the IEEE TRANSACTIONS ON MICROWAVE THEORY AND TECHNIQUES. He has been a member of organizing committees and technical program committees for many international conferences. He is a member of the German IEEE MTT/Antennas and Propagation Chapter Executive Board and the IEEE MTT-S Technical Coordinating Committees MTT-24, MTT-27, and MTT 29.